Surface structures by direct transform of electron diffraction patterns

2001 J. Phys.: Condens. Matter 13 10709

(http://iopscience.iop.org/0953-8984/13/47/312)

INSTITUTE OF PHYSICS PUBLISHING JOURNAL OF PHYSICS: CONDENSED MATTER

J. Phys.: Condens. Matter **13** (2001) 10709–10728 PII: S0953-8984(01)25926-8

Surface structures by direct transform of electron diffraction patterns

C Y Chang[1], I H Hong[1], Y C Chou[1] and C M Wei[2]

[1] Department of Physics, National Tsing-Hua University, Hsin-Chu, Taiwan 30055, Republic of China
[2] Institute of Physics, Academia Sinica, Nankang, Taipei, Taiwan, 11529, Republic of China

Received 19 June 2000
Published 9 November 2001
Online at stacks.iop.org/JPhysCM/13/10709

Abstract

We find that electron diffraction patterns can be directly inverted to provide three-dimensional atomic structures for the system studied. Depending on the scattering process, either holography or a Patterson inversion scheme is used. For diffraction patterns which were generated from a localized emitter source or predominantly by an inelastic-scattering feature like low-energy Kikuchi electrons, holography inversion is needed. The information obtained from Kikuchi electron holography includes the building blocks on the surface and their relative position to the atoms below the surface layer. On the other hand, for diffraction patterns generated predominantly by an elastic-scattering feature like low-energy electron diffraction (LEED), a Patterson inversion is needed. The information obtained from the Patterson transform of the LEED $I(E)$ curves is the relative positions of surface atoms to the atoms in underlying layers; no intra-layer information can be extracted with this method. High-fidelity and artifact-free three-dimensional atomic structures obtained by inversion of low-energy Kikuchi electron patterns and low-energy electron diffraction curves are presented. The results from the two inversion methods are complementary and can be used to construct or to discriminate the surface atomic structural models. The future of these direct methods by inverting diffraction patterns is discussed.

(Some figures in this article are in colour only in the electronic version)

1. Introduction

The determination of surface structure is the first step for thorough understanding of surface properties. Electron emission holography (EEH) [1–10] by direct transform of electron diffraction patterns has provided the three-dimensional (3D) relative positions between the atoms in the outermost layers of a surface of interest. Such information is very helpful to find out the most probable surface structure model. A good trial structure model, close to the actual structure, as the input of the refinement calculations will save much of the computing effort

before a realistic atomic structure can be determined. Many surface structural techniques need an approximate structure model as input for the refinement calculations. The dynamical low-energy electron diffraction (LEED) calculation [11] is one of the most important examples. However, guessing a test structure model for the dynamical LEED calculations is by no means a trivial process. It is a long-term goal for the surface structural technique to search for direct methods to image the three-dimensional atomic structures of the surface region.

The development of photoelectron emission holography suggested by Szoke [1], simulated by Barton [2] and extended to diffuse LEED holography by Saldin and de Andres [3] and to the Kikuchi electron pattern by Harp *et al* [4] has shed some light on this purpose. However, these early works with single-energy holography have only limited success because the electron multiple scattering effects or improper background subtraction have caused big artifacts mixed together with the real atomic images. The original methods to remove the artifact caused by the multiple scattering effects have been successfully proposed for photoelectron holography by Barton [5] and by Tong *et al* [6] and extended to diffuse LEED holography by Wei *et al* [7] and to Kikuchi electron holography (KEH) by Hong *et al* [8].

Recently a Patterson transform scheme like x-rays was successfully applied to correlated-thermal-diffuse scattering patterns by Abukawa *et al* [9], and to LEED $I(E)$ curves by Chang *et al* [10]. In the last decade, many direct methods by transforming diffraction patterns have been successfully developed. There is no doubt that all these direct methods will become widely used and combined with the conventional diffraction methods to solve the surface structures in the near future.

In this paper, we will show that the electron diffraction patterns can be transformed to obtain the three-dimensional atomic structures for the system studied. However, depending on the scattering process, either holography or a Patterson transform scheme is used. For diffraction patterns generated from a localized emitter source or predominantly by an inelastic-scattering feature like low-energy Kikuchi electrons, a holography transform is needed. On the other hand, for diffraction patterns generated predominantly by an elastic-scattering feature like low-energy electron diffraction $I(E)$ curves, a Patterson transform is needed. To prove our points, high-fidelity and artifact-free three-dimensional atomic images obtained by direct transform of low-energy Kikuchi electron patterns and LEED $I(E)$ curves will be presented. With the capability of imaging the surface characteristics such as adatoms, dimers and trimers and their relative positions to the underlying bulk atoms, Kikuchi electron holography is found to be an operable technique for determining the surface structure model, irrespective of the scattering power of the atoms in the surfaces of interest.

The rest of this paper is organized as follows. In the second section, we define the scattering processes for which holography transform and Patterson transform schemes are suitable. The details of two transform schemes are presented and the integral-energy phase-summing method to remove multiple scattering effects is briefly discussed. In section 3, the holographic transform scheme is adopted to obtain the atomic images from Kikuchi electron patterns. The results for a simple metal surface, a reconstructed silicon surface, a metal/silicon interface and a reacted silicon surface will be presented and discussed in detail. In section 4, the results of a Patterson transform of LEED $I(E)$ curves for the Sb/Si(111)-($\sqrt{3} \times \sqrt{3}$) R30° surface is summarized. Finally, the direct methods by transforming two kinds of diffraction pattern will be compared and their future applications will be discussed in section 5.

2. Patterson pattern and holography pattern

In this section, we will classify different kinds of electron diffraction pattern into two categories depending on their scattering process. We will also briefly describe the integral-energy

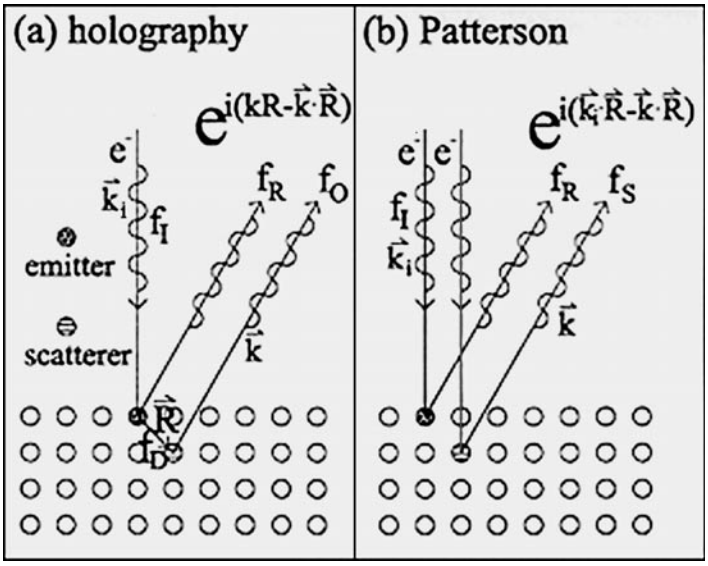

Figure 1. Schematic diagrams of (a) holographic diffraction process, (b) Patterson single scattering process.

phase-summing method [7] that successfully removes the multiple scattering effects and *thus make it possible to extract the information on the atomic pairs on the system by direct transform of the diffraction patterns.*

For different kinds of electron diffraction pattern or curve, in general, one can distinguish them into two categories: (i) for diffraction patterns which are generated from localized emitter source or dominated by an inelastic-scattering feature like core-level photoelectron or low-energy Kikuchi electron diffraction; (ii) for the diffraction patterns which are dominated by an elastic-scattering feature like electron correlated thermal diffuse scattering (CTDS) or low-energy electron diffraction $I(E)$ curves.

Generally speaking, the diffraction patterns, which are generated from a localized emitter source or through an inelastic-scattering process, can be viewed as holographic patterns. For example, consider the photoelectric effect that involves inelastic scattering of a photon to excite a core-level electron from the surface atom: the generated photoelectron diffraction pattern can be iterpreted as a hologram. The emission photoelectron wave from the emitted atom is regarded as a reference wave. As this reference wave is scattered by the nearby atoms, the scattered wave is the object wave. The interference between the reference and object waves forms a holographic pattern of surface atomic pairs. The Kikuchi electron, which lost its phase coherence with the incident beam after inelastic scattering process, can also be identified as a reference wave (f_R in figure 1(a)). The re-scattered wave of the singly scattered reference wave is the object wave (f_O in figure 1(a)). Thus it is expected that Kikuchi pattern is a holographic pattern, which could be transformed to yield three-dimensional atomic images. The holographic process with an external electron source was intrinsically a double scattering process, as depicted in figure 1(a).

On the other hand, there are elastic diffraction patterns involve no inelastic scattering event such as x-ray diffraction, CTDS patterns and LEED $I(E)$ curves. In x-ray crystallography, a single energy diffraction pattern is enough to produce the required Patterson function, since the multiple scattering could be neglected in x-ray diffraction. For CTDS patterns, which are

mainly contributed from the single scattering process, a multiple-energy Patterson function is also able to reveal atomic pairs on the surface [9]. For the LEED case, only the elastic scattering is involved. The major part of the scattering process, depicted in figure 1(b), is the single scattering process. Due to the fact that the single scattering process contributes largely to the modulation of the $I(E)$ curves, a Patterson transform should be used in direct transform of the LEED $I(E)$ curves [10], similar to that of x-ray scattering. Such a transform scheme is conceptually different from the holographic scheme [3, 7]. While for the LEED process, the multiple scattering process also contributes to the intensity modulation, we have to use the integral-energy phase-summing method (IEPSM) to eliminate the artifacts caused by the multiple scattering effects.

The IEPSM has been proved to be very effective to remove the multiple scattering effects and to reduce the artifacts, and has successfully applied to photoelectron [5, 6, 12], diffused LEED [7] and Kikuchi electron patterns [8, 13] to solve the surface structure. The formula for the holographic transform is

$$\boldsymbol{H}(\vec{R}) = \sum_{\hat{k}} \int g(\vec{k})\chi(\vec{k})\mathrm{e}^{-\mathrm{i}(kR-\vec{k}\vec{R})}k^2\,\mathrm{d}k \tag{1}$$

where $\vec{k}$ is the out-going electron wave vector, $\vec{R}$ is the relative position vector of the atomic pair, $g(\vec{k})$ is the window function, $\chi(\vec{k}) = (\boldsymbol{I}(\vec{k}) - \boldsymbol{I}_0(\vec{k}))/\boldsymbol{I}_0(\vec{k})$ is the normalized intensity modulation in which $\boldsymbol{I}_0(\vec{k})$ is a smooth varying function as an intensity background of $\boldsymbol{I}(\vec{k})$, and $\boldsymbol{H}(\vec{R})$ is summed over all diffraction directions. The resulting $|\boldsymbol{H}(\vec{R})|^2$ gives the atomic images of the surface atoms.

Here, we use photoelectron holography as an example to explain the reason for the success of IEPSM. For simplicity, let us assume an S-wave emitted from atom $\boldsymbol{E}$ at the origin, and only two nearby atoms i and j at $\vec{R}_i$, $\vec{R}_j$. If we consider scattering events which leave from atom i up to double scattering, then the diffraction intensity $\boldsymbol{I}(\vec{k})$ can be written as

$$\boldsymbol{I}(\vec{k}) = \left|1 + f_i(\vec{k}_i)\mathrm{e}^{\mathrm{i}(kR_i-\vec{k}\vec{R}_i)}\big/R_i + f_i(\vec{k}_{ij})f_j(\vec{k}_j)\mathrm{e}^{\mathrm{i}(kR_j+kR_{ij}-\vec{k}\vec{R}_i)}\big/R_jR_{ij} + \cdots\right|^2 \tag{2}$$

The reason for the success in removing the multiple scattering effects for IEPSM is because an exact opposite phase factor $-\mathrm{i}(kR - \vec{k}\vec{R})$ is introduced for the transform formula (1) to cancel the electron path difference $\mathrm{i}(kR_i - \vec{k}\vec{R}_i)$ between the reference wave and the object wave, therefore $\boldsymbol{H}(\vec{R})$ will become a maximum when we sum over a large momentum space of the diffraction data if (i) $\vec{R} = \vec{R}_i$ (the position vector of atom i relative to atom $\boldsymbol{E}$) and (ii) $f_i(\vec{k})$ is a relatively smooth function in the sampling $\boldsymbol{k}$-space. The condition where $f_i(\vec{k})$ is a smooth function is needed. As one can see, the contribution of the single scattering object wave $f_i(\vec{k}_i)e^{i(kR_i-\vec{k}\vec{R}_i)}$ to $\boldsymbol{H}(\vec{R})$ will become a summation of $f_i(\vec{k}_i)$ when $\vec{R} = \vec{R}_i$ and thus $\boldsymbol{H}(\vec{R})$ will become a maximum only if $f_i(\vec{k}_i)$ is a smooth function in $\boldsymbol{k}$-space. This is called the stable-phase condition. For the case of a photoelectron, $f_i(\vec{k})$ is the atomic scattering factor and there exist two smooth regions in the forward and backward scattering directions. This is the stable-phase condition needed. In the system where the multiple scattering is not or only a little involved, then single-energy holography might work.

For the system where the multiple scattering effects cannot be neglected, then many complicated factors like $f_i(\vec{k}_{ij})f_j(\vec{k}_j)$ need to be considered and included in $f_i(\vec{k}_i)$. This will certainly destroy the stable-phase condition needed for the transform and creating artifacts if only single-energy holography pattern is used. To separate or select the single scattering object wave from the multiple scattering effect, an easy solution is to extend the transform along the energy direction as well as the angular directions. With this extension, one can see from formula (2) that the path difference $\mathrm{i}(kR_j + kR_{ij} - \vec{k}\vec{R}_i)$ for a double scattering event will not

be cancelled by the opposite phase factor $-i(kR - \vec{k}\vec{R})$ even if $\vec{R} = \vec{R}_i$. So the contribution from the double scattering events will have very little contribution to the integration in formula (1). As a result, the multiple scattering contribution will be eliminated when the summation along the energy direction is included. This is the exact reason why the IEPSM is successful in removing the multiple scattering effect and thus makes the holographic transform becomes a powerful direct method.

Based on the same concept, the formula (1) for holographic transform can be generalized to the Patterson transform, that is

$$\boldsymbol{P}(\vec{R}) = \sum_{\hat{k},\hat{k}_i} \int g(\vec{k})\chi(\vec{k})\mathrm{e}^{-\mathrm{i}(\vec{k}_i\vec{R}-\vec{k}\vec{R})}k^2\,\mathrm{d}k \tag{3}$$

where $\vec{k}_i$ is the incidence electron wave vector. The phase factor in Patterson transform (3) is to account for the 3D interference effect of the singly scattered waves of incident electron beam. The results $|\boldsymbol{H}(\vec{R})|^2$ or $|\boldsymbol{P}(\vec{R})|^2$, transformed by holographic transform formula (1) or Patterson transform formula (3), are three-dimensional atomic images relative to the emitter (or the Patterson origin in the latter case).

As we will show later that IEPSM introduced here is very effective in eliminating the multiple scattering effects and producing high-fidelity and artifact-free atomic images either for holography patterns or for Patterson patterns; therefore, we believe and propose that all the diffraction patterns are able to be transformed to reveal the atomic structures for the system studied.

3. Kikuchi electron holography as a surface structure determining technique

In this section, we will demonstrate that KEH is a holographic technique generally applicable to all kinds of surface and an operable surface-structural technique with the results on a metal surface [14], a reconstructed silicon surface [15], a metal/silicon interface [16] and a reacted silicon surface [17]. After the first successful multiple-energy experiment on low index surfaces of silver crystal [14], Kikuchi electron holography has gone through four stages of development: (A) established as holography, (B) proved to be surface sensitive, (C) confirming the existing surface structure model and (D) determining a complex surface structure. In the following, we will briefly discuss the development in each stage.

3.1. Establishment of KEH

The KEH experiments are carried out in a μ-metal UHV analysing chamber equipped with a three-grid rear-view LEED optics. Kikuchi patterns are recorded with a frame-transfer charge-coupled device camera (12-bit digitized readout, 1024×1024 pixels) coupled with an optical lens ($f/0.85$). For each energy, the diffraction pattern is recorded a few times and averaged to increase the signal to noise ratio. The Kikuchi electron patterns are then transformed using the integral-energy phase-summing method to eliminate the multiple scattering contributions. The transform produces the atomic images which represent vectorial atomic positions of near-neighbour atoms measured from reference atoms. The information is averaged over all equivalent reference atoms. The reconstructed images, with high resolution, are high-fidelity three-dimensional images of atoms relative to an emitter on the surface.

Initial KEH studies on the (100) surface of silver crystal [14] have showed that 3D images of atoms within three layers down from the emitter can be obtained with high signal-to-noise ratio. However, there may exist some doubt on the applicability of KEH to heavy-atom systems which involve a strong electron–nuclear interaction. The KEH results shown in figure 2 for the

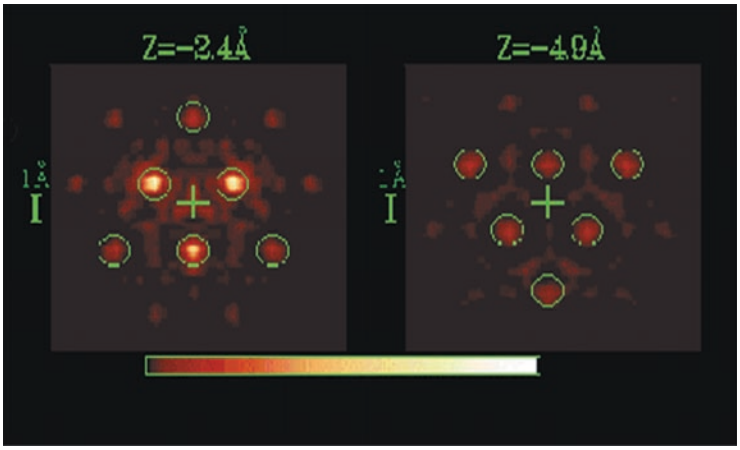

Figure 2. (a) and (b) show the top views of the reconstructed images of the atoms in the first and second atomic layers below the emitter.

Pt(111) surface should clear such a kind of doubt. The images reconstructed by transforming the normal incidence Kikuchi patterns using IEPSM can be directly compared with the relative positions deduced from the actual crystal structure of the Pt(111) surface. Figures 2(a) and (b) show the top views of the transformed images of atoms in the first and second atomic layers below the emitter. Sixteen Kikuchi patterns, with incident electron energies from 404 eV to 523 eV, were used in transforming the images. In figure 2(a), the images (local maxima of transformed image intensity) are at (1.4 Å, 0.8 Å, −2.5 Å) and its three-fold symmetric positions, which are in the first atomic layer below an emitter. The image positions correspond very well with the expected relative coordinates of a nearest neighbour to an emitter. There are additional local maxima at (0.0 Å, 3.1 Å, −2.2 Å) and its three-fold symmetric positions, which can be regarded as the atomic images of the second nearest neighbours of the emitter, in the first layer below the emitter. Figure 2(b) shows the transformed images in the second atomic layer below the emitter. The image positions are at (0.0 Å, 1.4 Å, −5.2 Å) and (2.7 Å, 1.4 Å, −4.9 Å), along with their three-fold symmetric repetitions. The corresponding expected atomic positions are at (0.0 Å, 1.4 Å, −4.6 Å) and (2.7 Å, 1.4 Å, −4.6 Å). The agreement between our image positions and the expected values is quite good. Therefore,we have demonstrated that even for a strong-scattering heavy-atom system like Pt, the multiple scattering effect is eliminated by IEPSM and the reconstructed atomic images have faithfully revealed the correct crystal structure.

3.2. Surface sensitivity

The KEH experiments with incident electron beam normal to the surface yield mostly the images of bulk atoms, because of relatively high contribution from the bulk atoms to the electron scattering, comparing to the surface atoms. In order to increase the surface sensitivity, one has to adopt the off-normal incident/detection configuration. In general, KEH experiments with 70° off-normal incidence is good enough for revealing the characteristic features to the surface. Here, we present the atomically resolved images of Au atoms in the trimers of the Si(111)$\sqrt{3} \times \sqrt{3}$ R30°–Au system [16] as an example to illustrate the surface sensitivity of KEH.

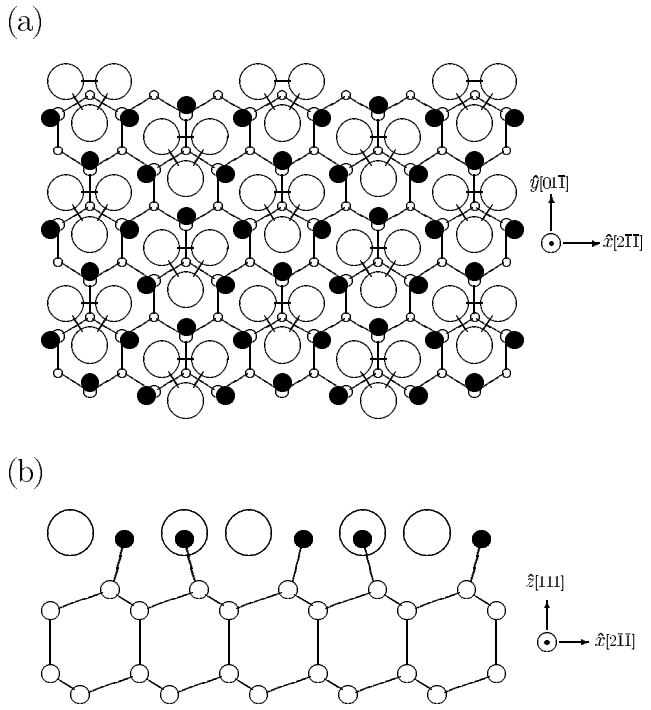

Figure 3. Schematic (a) top view and (b) side of the CHCT model for Si(111)–$\sqrt{3}$-Au. The largest circles in (a) and (b) represent Au atoms. All other circles represent Si atoms.

The $\sqrt{3} \times \sqrt{3}$ R30° (henceforth $\sqrt{3}$) structures of noble metals Ag and Au on Si(111) have been the subject of particularly intense studies because of the complexity of the atomic arrangements at the interface [18]. In each case, the adsorption of the metal atoms induces extensive surface restructuring—the top-layer Si atoms are completely peeled off and replaced by the metal atoms. The $\sqrt{3}$ periodicity is formed by subsequent rebonding of the metal atoms with Si atoms in the layer below [19–21]. As explained by Ding *et al* [22] in the Au-$\sqrt{3}$ system, the Au–Au bond is stronger than either the Au–Si or Si–Si bond. This results in Au trimerization in the surface layer and the Si lattice below distorts to bond to the Au trimers (see figure 3). The structure of this surface is known as the conjugate honeycomb-chained-trimer (CHCT) model.

In order to image the Au trimer atoms, a grazing-incidence-beam-backscattering detection geometry is used to increase the surface sensitivity. The crystal is rotated so that the LEED gun is pointed along the $[-211]$ direction at 80° from the surface normal. In this scattering geometry, the majority of the collected Kikuchi electrons come from backscattering within the first two layers of the sample. Also, the much stronger scattering factor of Au compared to Si further enhances the contribution from the Au layer. In figure 4(a), we show a Au trimer (atoms labelled 1, 2 and 3) and its nearest neighbour trimer (atoms labelled 4, 8 and 9) in the CHCT model. Atoms 5, 6 and 7 are second-layer Si atoms, 0.46 Å below the plane of the Au atoms. In Kikuchi electron imaging, every atom acts as a reference atom. Figure 4(c) shows E_1 as the reference atom, from which the nearest-neighbour atoms S_2, S_3 and S_5 are imaged along backscattering directions. Similarly, figures 4(b) and (e) show atom E_2 (E_3) as the reference atom, imaging atom S_4 and S_8 (S_4 and S_9) in the next trimer. Figure 4(d) shows

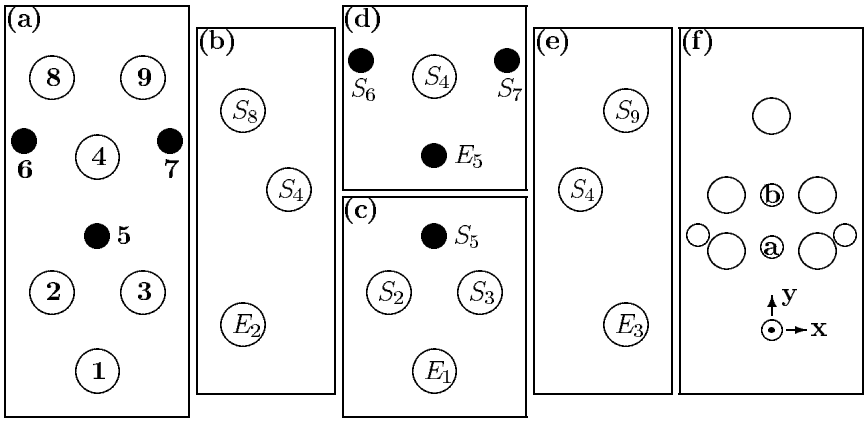

Figure 4. Illustration of expected atomic images from glancing-angle Kikuchi electron holography. The incident beam travels from bottom to top. (a) Top view of Au trimer (labelled 1, 2 and 3) and its nearest-neighbour trimer (labelled 4, 8 and 9); the circles labelled 5, 6, 7 represent the Si atoms; panels (b) to (e), emitter–scatterer pairs which contribute to the hologram. (f) The expected atomic images from all inequivalent emitter–scatterer pairs.

the second-layer Si atom E_5 imaging Au atom S_4 and Si atoms S_6 and S_7. Translation of the four reference atoms to a common origin results in a predicted image depicted in figure 4(f), if the CHCT model is correct.

The colour images in figure 5 are the actual atomic images obtained by reconstructing 32 grazing incidence (80° from normal) Kikuchi electron patterns in the energy range 196 to 389 eV. Referring to figure 5, at the emitter plane (lower left panel), the two bright spots 2.78 Å from the origin are Au atoms in the same trimer and the other bright spot 6.63 Å due north from the origin is Au atoms in the neighbour trimer. The two spots 4.43 Å away are equally well resolved and free from streaking. This is direct evidence that the Au trimers are mostly well ordered. Further evidence of ordered trimers on the surface is the sharp spot 2.40 Å (lower right panel) due north of the origin. According to figure 4(d), this spot is the image of Au atom 4 seen from the second-layer Si atom 5. The sharp spot 4.20 Å (top centre panel) due north of the origin is the image of Si atom 5 seen from the top-layer Au atom 1. The isotropic shape of these two images and the lack of streakiness of the spots suggest that the Au trimers are well ordered with respect to the second-layer Si plane. The image spots of figure 5 in three-dimensional space have one-to-one correspondence to figure 4(f) and this proves the CHCT model is the correct model for an Au-$\sqrt{3}$ Si(111) surface.

The surface sensitivity is essential for KEH to develop as a surface structural technique, and is demonstrated in the studies of the dimers on the Si(100) 2×1 surface, the adatoms and dimers on the Si(111) 7×7 surface and the trimers on the Si(111)$\sqrt{3}\times\sqrt{3}$R30°–Sb (or Au) surface. Not only the characteristic features on the outermost layers, but also their relative position to the bulk atoms under the surface layers are observed. The highly surface sensitivity of KEH is advantageous in discriminating the surface atomic-structure models.

3.3. Confirmation of surface structure model

From the above example for the Au-$\sqrt{3}$ system, one can see that Kikuchi electron holography is particular useful in finding the building blocks on the surface, and therefore to rule out or confirm the proposed surface structural models. Here, we will present the results of

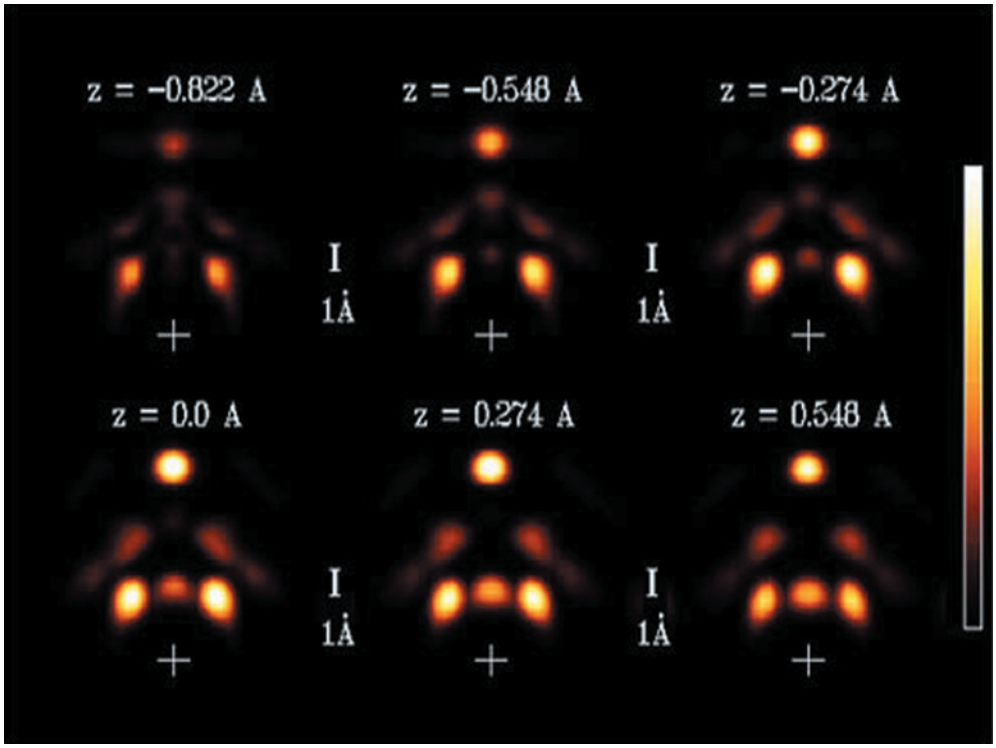

Figure 5. Holographic images of Si(111)-(3×2)surface. The incident e-beam is 80° from the surface normal and is along [−211]. Six atomic images are cut in the planes from $z = -0.822$ Å to $z = +0.548$ Å in a step of 0.274 Å. The image spots have one-to-one correspondence to figure 4(f), and thus prove the CHCT model is the correct model for the Au–$\sqrt{3}$ Si(111) surface.

confirmation of the structural model of the Si(113) 3×2 surface (as the puckered tetramer model) by transforming the Kikuchi electron patterns [15].

The surface structure of reconstructed Si(113) surfaces has been studied for many years. Various experimental techniques, such as low-energy electron diffraction, scanning tunnelling microscopy, high-resolution electron-energy loss spectroscopy, surface-x-ray-diffraction etc have been used to determine the surface structure [23–28]. However, no consensus has been reached. One class of commonly mentioned models is the Ranke (3×1)-2 model (R-model) (figure 6(a)) and its modified versions [23]. Another is the recently proposed interstitial model (D-model) (figure 6(b)) by Dabrowski *et al* [24]. The R-model could be described by the dimerization and the adatom on the surface, which are known to be effective to reduce the number of dangling bonds, and thus to lower the surface energy. Wang *et al* [29] conducted an *ab initio* pseudopotential total-energy-minimization calculation and they arrived at the oppositely puckered model (figure 6(c)), which is topologically similar to the R-(3×1)-2 model. The D-model, which is described by an insertion of an interstitial atom (I.A. in Figure 6(b)) with sixfold coordination, was first introduced to explain the scanning tunnelling spectroscopy (STM) images, and claimed to be energy minimized by an *ab initio* theory [24].

In order to clear up the controversial model of the reconstructed Si(113) surface, we perform the Kikuchi electron holography studies for this system. From what we have learned above for the Au-$\sqrt{3}$ system, one can expect the image spots for the Ranke model, interstitial model and oppositely puckered model will be very different and easy to resolve using the

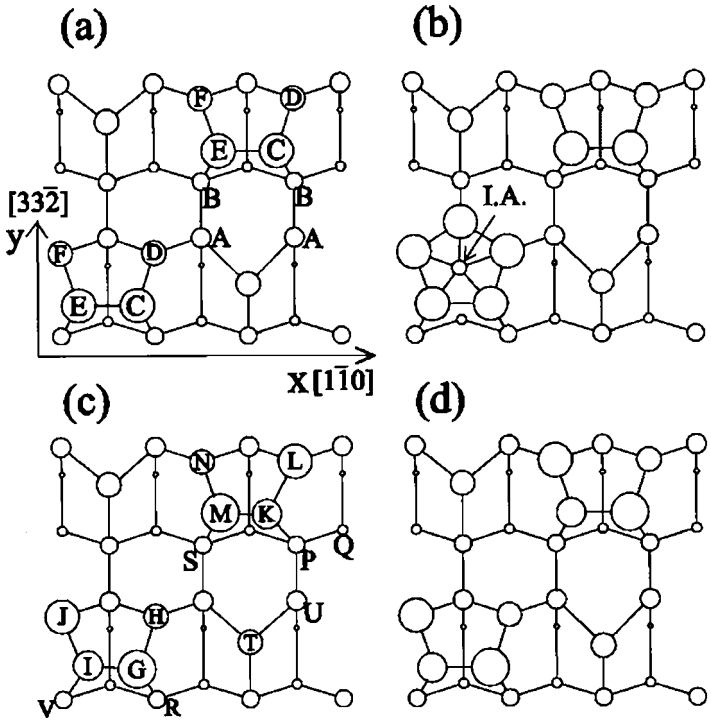

Figure 6. Top view of Si(113) structure models: (a) the R-(3×1)-2 tetramer model, (b) interstitial D-model, (c) puckering tetramer (3×2) model, (d) puckering tetramer (3×1) model. The smaller circles represent the atoms that are farther from the vacuum.

Kikuchi electron holography technique. For example, using a glancing incidence detection geometry where the electron beam is injected along the [33-2] direction, the expected image spots for the oppositely puckered model (figure 6(c)) will be the atomic pairs of I–J, G–H, M–N and K–L, thus creating the atomic image spots above and below the emitter plane ($z = 0$ *Å* plane). On the other hand, the Ranke model will only conduct image spots below the emitter plane, while the interstitial model will conduct image spots above/below and at the emitter plane. Therefore, the real image spots by transforming experimental Kikuchi electron patterns will unambiguously tell us which one is the correct model for the Si(113) 3×2 surface.

Figure 7 shows the reconstructed atomic images of the Si(113)-(3×2) surface by direct transform of Kikuchi patterns with incident e-beam 70° from the surface normal and along the [33-2] direction. All the images are viewed in the planes parallel to the surface. Figures 7(a) and (b) are in the planes below the emitter for (a) $z = -0.822$ *Å* and (b) $z = -0.274$ *Å* respectively. Figure 7(c) is in the plane above the emitter for $z = +0.548$ *Å*. Note the image spots 1 to 5 are clearly in the backward scattering configuration. As a reference, the image spot 3, with strongest intensity, is the holographic image caused by the Si atom pairs at bulk sites such as the atoms A and B (figure 6(a)), where A is considered to be an emitter and B is a scatterer. The resolution (∼0.6 Å) of the reconstructed images could be attained by the image size (full width at half maximum) of spot 3. The position of spot 3 is compared well with the expected position.

The image spots 1, 2 at (1.0 Å, 2.1 Å, −0.9 Å) below the emitter plane and image spots 4, 5 at (0.9 Å, 2.3 Å, +0.5 Å) above the emitter plane must be related to the surface reconstructed

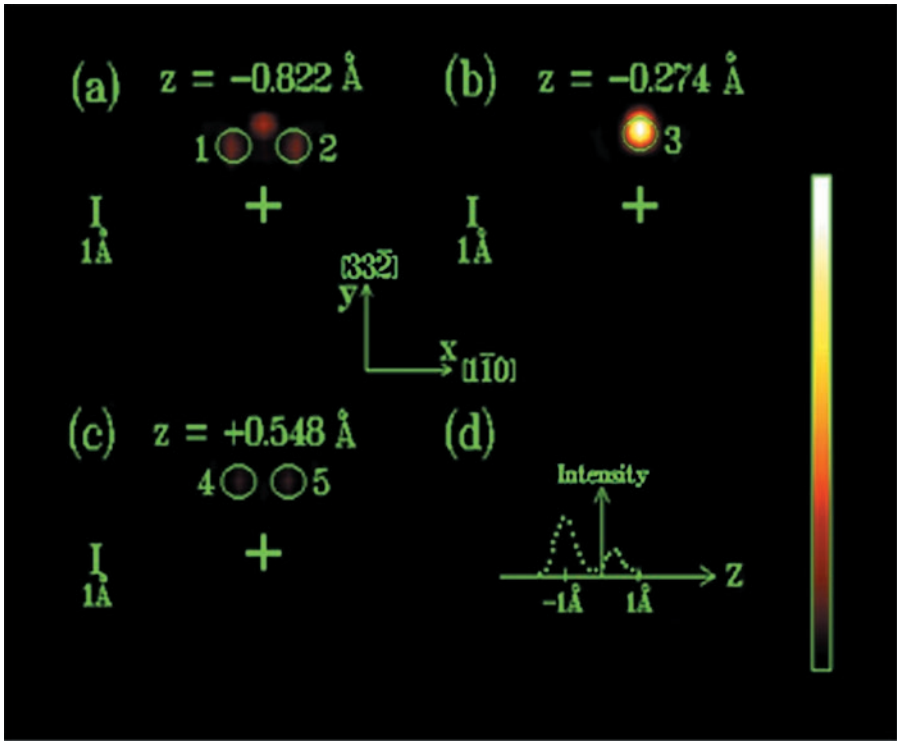

Figure 7. Holographic images of the Si(113)-(3×2)surface. The incident e-beam is 70° from the surface normal and is along [33-2]. (a)–(c) Atomic images in the planes for $z = -0.822$ Å, $z = -0.274$ Å and $z = +0.548$ Å, respectively. (d) The intensity profile along the line linking the image spots 1 and 4. The image spots 1, 2, 4, 5 can be understood as holographic images from two oppositely puckered tetramers (figure 6(c)).

atoms, since the holographic image between the bulk atom pairs will result only in the integral multiples of 1.92 Å for the x-coordinate. These four spots cannot be accounted for by the R-model, nor by the D-model. In the R-model, the two dimerized atoms, together with the two nearby surface atoms, form an inclined coplanar tetramer structure (atoms C, D, E, F in figure 6(a)). Considering the dimerized atom C (or atom E) as the emitter and the nearby surface atom D (or atom F) as a scatter, one should observe two images at (0.8 Å, 2.2 Å, −0.4 Å) obtained from *ab initio* total energy calculations [30]. These two images seem to be able to explain our reconstructed atomic image spots 1, 2 in figure 7. However, no other atomic pairs in the R-model could be found to fit our reconstructed image spots 4, 5, which are situated in the image plane above the emitter. Thus, the R-model is insufficient to explain our experimental data. In the interstitial D-model, a flat pentagon is the building block on the surface, while an interstitial atom (with sixfold coordination) is inserted beneath the pentagon (figure 6(b)). If this D-model is right, we should have observed some atomic images near $z = 0.0$ Å. However, no image spots were found. In our KEH images, neither the image from the atomic pair in the pentagon nor the image from the atomic pair between the pentagon atoms and the interstitial atom are observed. So we rule out the D-model as a candidate to explain our KEH images.

The facts that the image spots 1, 4 (or spots 2, 5) have similar x, y coordinate values and are on the opposite sides of the $z = 0$ (emitter) plane guide us to the conception that

the tetramer is puckered, i.e. the puckered tetramer (atoms G, H, I, J in figure 6(c)) can be obtained by buckling down the atoms E, D and buckling up the atoms C, F in figure 6(a). The reconstructed image spot 2 is the holographic image as viewing from atom G to H, and spot 4 is the holographic image viewing from atom I to J, while the image spots 1, 5 come from another oppositely puckered tetramer (atoms K, L, M, N). The puckering tetramer model was first initiated by Wang *et al* through *ab initio* energy-minimization calculations [29]. From the image shown in figure 7, we can infer that two kinds of tetramer, puckering in different directions, exist on the Si(113)-(3×2) surface. Indeed, the reconstructed images of KEH fit well with the puckered tetramer model. As a matter of fact, we found a published high-resolution STM result [31] that clearly resembled the puckered tetramer model, although, in their paper, the authors did not explain their results according to the puckered tetramer model.

3.4. New surface structure determination

Though KEH is useful in confirming an exist surface structural model, for a complex surface a complete structure is not obtained only by KEH. A combination of KEH with other surface techniques will be helpful and necessary for a more complete structural determination. Here we will present a combined study of KEH, STM and *ab initio* total energy calculations on the complex 8×8 surface of silicon nitride film growth on an Si(111) surface.

Silicon nitride (Si_3N_4) film has been widely used for high-temperature ceramic and microelectronic applications due to its unique electrical, optical, mechanical and chemical properties. A better understanding of the structure and growth mechanisms of Si_3N_4 films deposited on Si is necessary. Despite its importance, at present, there is a lack of complete understanding on either the surface or interface structure of the Si_3N_4/Si system. Si_3N_4 films deposited on Si are usually amorphous. However, as an exception, a coherent $Si_3N_4(0001)/Si(111)$ interface can be formed using the thermal nitridation process. This is related to a nearly perfect lattice match: the 2×2 cell of the Si(111) surface ($a_{Si} = 3.84$ Å) is only ∼1.1% bigger than the unit cell of $\beta-Si_3N_4(0001)$ ($a_{\beta\text{-}Si_3N_4} = 7.61$ Å) [32]. Several contradicting structural models have been proposed so far for the intriguing $Si_3N_4(0001)/Si(111)$-(8×8) (denoted as '8×8' structure in this paper) surface, although none of them are conclusive [33–36]. Compared with Si(111)-7×7, the '8×8' structure is more complicated in two aspects: (1) the unit cell is ∼14% larger, and (2) there are two different atoms. The determination of this surface remains as a great challenge of the surface science community.

The observation of the adatoms with ∼10–11 Å separation in the first atomic layer of the surface by direct transform of Kikuchi patterns plays a key role in determining the structure. Figure 8 shows the reconstructed images using KEH study at $z = 0$ Å (indicating that the emitters and the scatterers are in the same atomic plane) for three glancing angles of incidence (30°, 60° and 70°). The brightest reconstructed image spots (3) marked with circles in figures 8(b) and (c) appear at [5.0 Å, 8.2 Å, −0.5 Å] and [5.5 Å, 8.7 Å, 0.0 Å], respectively. There is no similar atomic pair in smaller incidence angle KEH, for example 30° in figure 8(a). As we have shown in the previous works, choosing a bigger incident angle of the electron beam can greatly enhance the sensitivity of KEH on the surface. Therefore the atomic pairs we found at 60° and 70° are mostly originated from the surface. The distance between the emitter and the scatterer of the image spot 3 is about 10–11 Å. This distance is close to the periodicity of the '3/8×3/8' structure observed in many previous works, but none of them could provide a sufficient explanation [33, 36, 37]. Meanwhile, in the original LEED patterns, the 3/8th fractional index spots are always much brighter than the others and persist as long as there is 8×8 surface structure. Therefore, this superstructure of adatoms is intrinsic, so does not depend on the purity of NH_3 gas or the preparation conditions as mentioned by Wang *et al* [34].

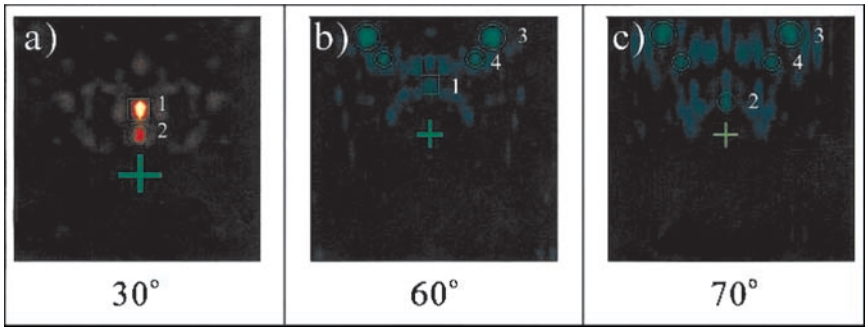

Figure 8. The atomic images reconstructed from KEH patterns at $z = 0$ Å for the incident angles of (a) 30°, (b) 60° and (c) 70°. The cross marks the position of an emitter.

For all of our KEH measurement, the incident electron beam was following the [11-2] direction of the Si(111) substrate and all of the reconstructed atomic pairs including those in figure 8 appeared symmetric. This fact suggests that the Si_3N_4 rest layer has a mirror symmetry along the [11-2] direction of the Si(111) substrate. Indeed, the Kikuchi patterns along this direction show a mirror symmetry as well as three-fold rotational symmetry. The bulk-terminated Si_3N_4 model proposed by Wang *et al*, however, cannot explain the existence of a mirror symmetry that is clearly shown even in their LEED image. To confirm this argument, we performed KEH measurement normal to [11-2] by rotating the sample by 90°, and most of the identified atomic pairs appeared asymmetric (not shown). These KEH results, combined with the results by scanning tunnelling spectroscopy that the $8/3\times8/3$ ordering spots in the occupied state images correspond to the nitrogen adatoms [17], provide us with the reason to seek a new atomic structure model of this complicated surface.

The proposed atomic model is similar to the Si(111)-7×7 DAS model, which consists of an upper adatom layer which caps the rest layer beneath. The rest layer before relaxation has a 1×1 unit cell of Si_3N_4 as shown in figure 9(a). Repeated 1×1 unit cells form a circular feature, which has three high-level nitrogen atoms, and three low-level nitrogen atoms on the alternate corners of a circle. On top of this rest layer we included the nitrogen adatoms with the periodicity of 10.2 Å as suggested by the KEH images and performed *ab initio* total energy calculations using the Vienna *ab initio* simulation package (VASP) [38]. Up to now, no total energy calculations for this surface structure have been attempted because of the extreme difficulty of handling such a large number of two different kinds of atom.

Figure 9(b) shows the result of total energy calculation with adatoms. The green and redsolid circles are silicon and nitrogen atoms, respectively. Adatoms are marked by bluesolid squares. As one can see in the left half of the diamond unit cell, the three adatoms (1, 5 and 6) that lie on the top-site of tetrahedral bonding in the restlayer do not disturb the basic feature of the restlayer underneath. However, in the right half of the unit cell, the adatoms sit approximately on the hollow site of the restlayer and have atomic bonds with two nitrogen atoms, and the restlayer structure near these adatoms is extremely distorted. This uneven relaxation around adatoms results in the formation of a big diamond-shape unit cell and the asymmetry of the left and right halves of the unit cell. One unit cell is marked with the solid line. In this figure each cell has a mirror symmetry axis along the long diagonal axis of the diamond as well as three-fold rotational symmetry.

Compared with the atomic coordinates in our model, the atomic image spot 3 observed in figure 8 can be identified as the atomic pairs between adatom (8–4) pair with the coordinate

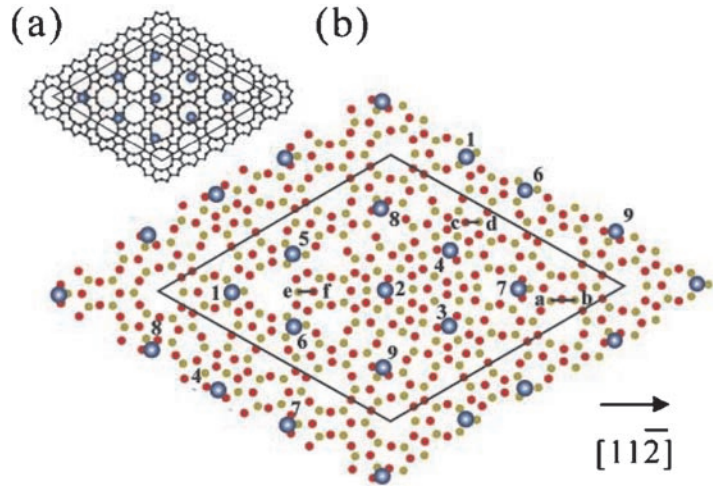

Figure 9. The proposed 8×8 atomic model before (a) and after (b) the total energy relaxation. The large blue solid circles in (a) and (b) are nitrogen adatoms on the topmost layer. The small red (green) solid circles are nitrogen (silicon) atoms on the rest layer.

at [4.6, 7.7, −0.5] (Å). The atomic image spot 4 at [3.8, 6.5, 0.5] (Å) in figures 8(b) and (c) can be assigned to the atomic pair between adatoms (1–6) with the coordinate at [3.9, 6.8, 0.0] (Å). The weak features in figure 8 can also be assigned to the atomic pairs in our model. Within the accuracy of KEH, the agreement is very good.

More than 30 reconstructed atomic pairs were successfully assigned compared with the theoretical results. The image spot 2 in figure 8(a), which locates at [0.0, 1.64, −0.85] (Å) can be compared with the Si–N atomic pairs with tetrahedral bonds, such as (c–d) [0, 1.55, −0.68] (Å) or (e–f) [0, 1.46, −1.1] (Å). We can calculate the Si–N tetrahedral atomic bond length from these pairs; this is the most prevailing pair in the rest layer. The calculated bond length is 1.70–1.83 Å, which is in excellent agreement with the previously reported results, 1.68–1.78 Å [35, 39].

In summary, we have shown that the direct transform of Kikuchi electron patterns, with glancing incidence detection configuration, produces direct evidence that the Au trimers are arranged in the CHCT configuration for the Au-$\sqrt{3}$ on Si(111) system, that the Si(113) (3×2) surface is oppositely puckered and also the N adatom arrangement on the Si_3N_4 (0001)/Si(111)-(8×8) surface. In the Kikuchi electron transform, both surface and bulk information can be obtained by changing the angle of incidence. Only the scatterers, within the electron mean free path, lying to the far side of a reference atom from the electron gun are imaged. Kikuchi electron patterns are easily collected using laboratory-based equipment and data acquisition takes only a few seconds per pattern. The systems presented here are some examples where the superior resolution of the method allows an unambiguous interpretation of the images even in the presence of multiple, inequivalent reference atoms.

4. Patterson transform of LEED *I*(*E*) curves of the Si(111)-($\sqrt{3} \times \sqrt{3}$)–Sb surface

In this section, we will present the high-fidelity atomic images of the Si(111)-($\sqrt{3} \times \sqrt{3}$) R30°–Sb surface by Patterson transform of its LEED *I*(*E*) curves [10]. We will show that transform of the LEED *I*(*E*) curves of the integral-order spots gives the images of bulk atoms,

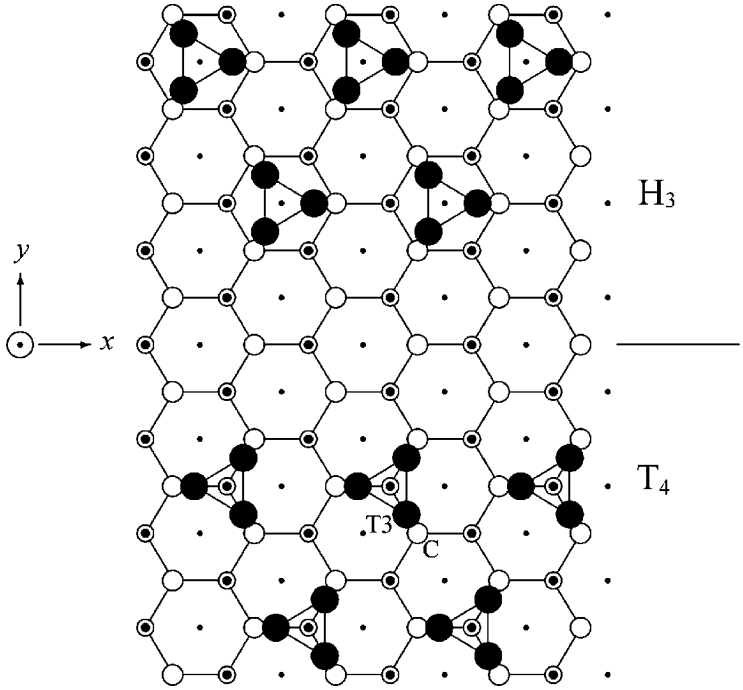

Figure 10. Structure models of Sb-$\sqrt{3}$ surface. The milk-stool T_4 and H_3 models are shown respectively.

whereas transform of the fractional-order LEED $I(E)$ curves reveals the surface structures. For the LEED experiment, the diffraction direction $\vec{k}$ is limited to the discrete spots determined by translation symmetry of the sample. The structural information contained in integer-order and fractional-order beams is different. Taking the Si(111)-($\sqrt{3} \times \sqrt{3}$) R30°–Sb surface as an example, the integer-order LEED spots are mostly due to the electron scattering of atoms with the 1×1 substrate translation symmetry, while the fractional-order spots of the Si(111)-($\sqrt{3} \times \sqrt{3}$) R30°–Sb surface must involve at least one scattering with the surface atoms having $\sqrt{3} \times \sqrt{3}$ superstructure translation symmetry and thus the surface sensitivity is guaranteed.

After deposition of Sb atoms on the Si(111) surface, the adsorbed Sb atoms change the surface from 7×7 structure into Si(111)-($\sqrt{3} \times \sqrt{3}$) R30°–Sb (abbreviated as Sb-$\sqrt{3}$ hitherto) structure [40–42]. Some possible structural models, e.g. milk stool T_4, milk stool H_3 (shown in figure 10), and bridge T_4, bridge H_3 structure models were proposed to explain the Sb-$\sqrt{3}$ surface. For these structure models, the Sb-trimer was the basic surface building block, however, with different rotation or different register sites on the surface. We will show by comparing atomic images of transform of integer and fraction order spots of LEED $I(E)$ curves that the milk stool T_4 model is the correct structural model.

In our experiment, a rear-view LEED optics is used to display the LEED patterns, which are then recorded by a charge coupled device camera. The energy range used for transform is from 70 eV to 250 eV. The number of LEED $I(E)$ curves used for the transform is limited by the opening angle (104°) of the LEED optics. Only the $I(E)$ curves with sufficiently large wave vector $\boldsymbol{k}$-range ($\geqslant$1.5 au) are used for the transform. The reconstructed atomic images are not sensitive to the inner potential chosen for the transform. Since it is the intensity modulation $\chi(\vec{k})$ that contains the structure information, a low-order polynomial fit of $I(E)$ is used as the

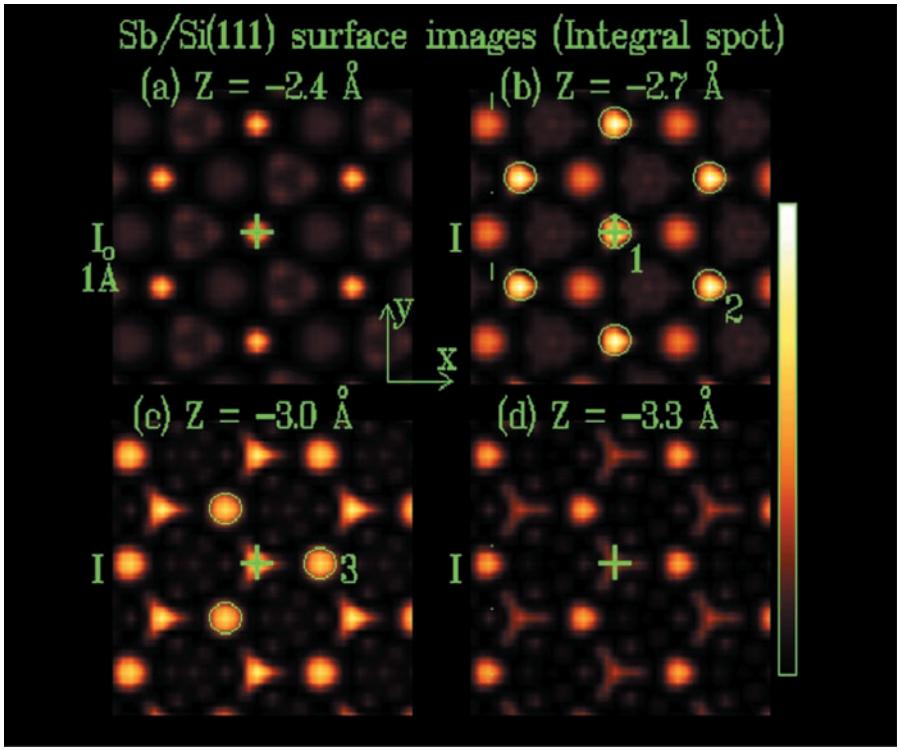

Figure 11. Patterson transformed images of integer-order LEED spots of the Sb-$\sqrt{3}$ surface of normal incident configuration (a), (b), (c): top views of atomic images of z-planecuts for (a) $z = -2.4$ Å, (b) $z = -2.7$ Å, (c) $z = -3.0$ Å and (d) $z = -3.3$ Å, respectively. The cross symbol marks the projection of the origin on the z plane. The centre of the circle marks the correct relative position of the atomic pair.

intensity background. Improper subtraction of the intensity background will produce a huge peak at the Patterson origin in the transformed images.

In figure 11, we show the reconstructed atomic images of integer-order LEED $I(E)$ curves of the Sb-$\sqrt{3}$ surface with the Patterson transform scheme. The bright spots are the 3D images of the atomic pair with one atom situated at the Patterson origin. The atomic images fit quite well (within 0.3 Å) with the relative positions between the atoms in the bulk structure. The mean free path of an electron of energy 200 eV is roughly 10 Å and the electron will probe roughly three atomic bilayers in the bulk region. The assignment of the reconstructed atomic images is referred to the structure model shown in figure 10.

The multiple scattering process exists in each $I(E)$ curve, and a double scattering wave can be considered as holographic object wave with respect to a single scattering wave, see figure 1(a). Therefore, it is interesting to see if the holographic transform of LEED $I(E)$ curves will reveal the atomic structures for the system. We find that the atomic images, obtained by the holographic transform, result in large deviation in z-coordinate of the image spots from the bulk values ($\geqslant$1.0 Å). Thus we can conclude that the Patterson transform is the correct transform scheme for the integer-order beams, and the single scattering process in the bulk region contributes mostly to the intensity modulation in the integer-order LEED $I(E)$ curves.

The deviation of the resulted images of holographic scheme could be understood by comparing the two phase factors $e^{-i(kR-\vec{k}\vec{R})}$, $e^{-i(\vec{k}_i\vec{R}-\vec{k}\vec{R})}$ in formulae (1) and (3), respectively.

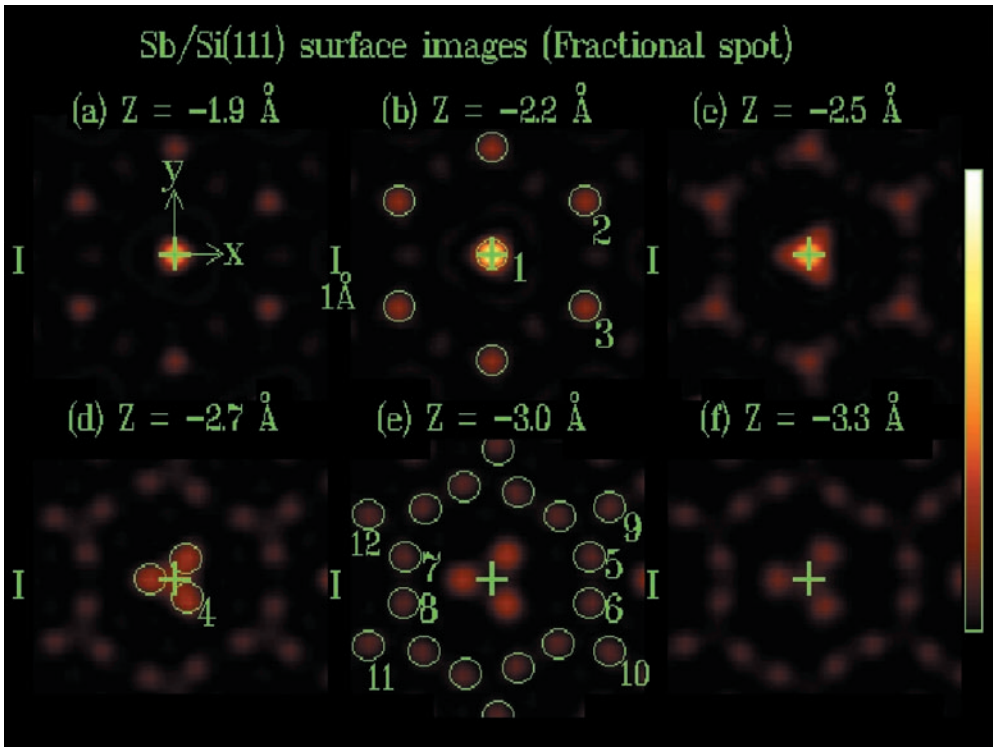

Figure 12. Patterson transformed images from LEED $I(E)$ curves of fractional-order spots of the Sb-$\sqrt{3}$ surface. (a)–(f) are the top views of atomic images of four z-plane cuts of -1.9, -2.2, -2.5, -2.7, -3.0 and -3.3 Å, respectively. The centre of the circle marks the correct relative position of the atomic pair.

The two phase factors differ by a multiplier term $\exp[\mathrm{i}(kR - \vec{k}_i\vec{R})]$. For the normal incidence configuration, where $\vec{k}_i = (0, 0, -k)$ and $\vec{R} = (x, y, z)$, the difference term results in $\exp[\mathrm{i}k(R + z)]$. Thus, for the atomic pairs where the scatterer is right beneath the emitter, i.e. $z = -R$, there is no difference in phase factors for both Patterson and holographic transforms, and the two transforms will yield the same results. While for the atomic pairs not in the strictly backward direction ($-z$ direction), as position vector $\vec{R}$ of the atomic pair points gradually away from the incident direction, the difference in the atomic images by the two transform schemes will gradually come out and become larger.

In order to image the surface atomic pairs, we have to use the fractional-order LEED $I(E)$ curves. The surface sensitivity was guaranteed by using the fractional-order beams. Shown in figure 12 are the atomic images inverted from the fractional-order LEED $I(E)$ curves of the Sb-$\sqrt{3}$ surface. Apart from the atomic images of bulk atom pairs (spots 1, 2 and 3), the atomic images 4–12 give the relative positions between the adsorbed Sb atom and the underlying bulk Si atom.

Special attention should be paid to the image spot 4, with coordinates (0.4 Å, -0.6 Å, -2.7 Å). Among the various proposed structural models of the Sb-$\sqrt{3}$ surface (see figure 10), only the building block of the milk stool T_4 model can explain the image spot 4. This spot can be understood as the holographic image as viewing from T3 to C, as shown in figure 10. Thus, based on the result of direct inversion of LEED $I(E)$ curves, we support the milk stool T_4 model as the right structural model for the Sb-$\sqrt{3}$ surface.

The holographic inversion was also applied to the fractional-order beam of the Sb-$\sqrt{3}$ surface. The reconstructed atomic images reveal obvious shifting of atomic images, except the atomic images of the atomic pair aligned with the z-axes. This shifting is also observed in the holographic inversion of LEED $I(E)$ curves of clean Si(113) surfaces. With the experimental results of the pure Si(113) surface and the Sb-$\sqrt{3}$ surface, we come to the conclusion that the LEED pattern should be identified as a Patterson pattern. That is the Patterson inversion is the correct inversion scheme for both direct inversion of LEED $I(E)$ curves of the pure Si surface and the Si surface with adsorbed heavy atoms.

The STM has been applied to solve this Sb-$\sqrt{3}$ surface [42]. Although the trimer structure could be observed, the registration site could not be determined. In our previous off-normal KEH study of the Sb-$\sqrt{3}$ surface [43], the atomic images of the trimer, as well as relative position between the trimer atom to the bulk atom, were imaged. The results of Patterson inversion of LEED $I(E)$ curves are consistent with the results of the KEH study of the Sb-$\sqrt{3}$ surface. Although the atomic images obtained by KEH and Patterson inversion of LEED $I(E)$ curves are quite different, both results support the milk stool T_4 structure model.

In summary, we have demonstrated that the correct transform scheme for the LEED $I(E)$ curves of Sb-$\sqrt{3}$ surface is the Patterson scheme. Although the multiple scattering process exists in each $I(E)$ curve, the IEPSM filters out the multiple scattering effects, and only the kinematical components remain. In general, a transform of the LEED $I(E)$ curves of integral-order spots gives the images of bulk atoms, whereas a transform of the fractional-order LEED $I(E)$ curves shows high surface sensitivity.

5. Outlook for the future of transforms of electron diffraction patterns

We classify all different kinds of diffraction pattern into two categories: (i) holography patterns where a local source of the emitted wave exists; (ii) Patterson patterns where the external incident wave is diffracted in a phase coherent way. The difference between the Patterson and holographic ideas is clearly seen in figure 1. For a holographic process, a local source of the emitted wave, which has lost its phase coherence, is needed. Thus, the holographic transform should work and apply for Kikuchi electron and photoelectron patterns, whereas in a Patterson process the externally incident wave is diffracted in a phase coherent way. The Patterson transform should be used for x-ray diffraction and electron correlated thermal diffuse scattering. As for LEED, the single elastic scattering dominates over the various kinds of multiple scattering, and thus a Patterson transform is needed to reconstruct the LEED $I(E)$ curves.

In any situation the IEPSM can effectively eliminate the multiple scattering effects, and reconstruct high-fidelity, artifact-free atomic images from all different diffraction patterns with equations (1) and (3), respectively. We believe and propose that all the diffraction patterns can be directly transformed to provide three-dimensional atomic structures for the system studied. We have proved this fact by presenting high-fidelity and artifact-free 3D atomic structures transformed from low-energy Kikuchi electron patterns [15, 16] and low-energy electron diffraction $I(E)$ curves [10].

For the LEED patterns, which are better described as Patterson patterns, a Patterson transform is used to obtain the 3D atomic structure of the system. The Kikuchi patterns, where the electron encounters at least one inelastically scattered event, can be identified as holographic patterns, thus a holographic transform has to be adopted to obtain the atomic images. The resolution achieved is about 0.6 Å for both the Patterson transform of LEED $I(E)$ curves and Kikuchi electron holography. The surface sensitivity of LEED $I(E)$ curves is guaranteed by using fractional-order beams, where the scattering process involves at least one

surface atom, for the transform, while for the KEH a glancing incidence configuration must be used to increase the surface sensitivity. From the determination of the structural model of Si(111)-$\sqrt{3} \times \sqrt{3}$–Au, Si(113)-3 $\times$ 2 surfaces and Si(111)-$\sqrt{3} \times \sqrt{3}$–Sb, it is obvious that direct transform of LEED $I(E)$ curves and Kikuchi patterns are capable of obtaining the surface structure model of an unsolved surface structure. What we have obtained in direct transforms of LEED $I(E)$ curves are the relative positions between the surface atoms and the underlying atoms of the next layer, and it is difficult to image the building block in the same surface layer. However, the building block on the surface can be easily imaged with off-normal Kikuchi electron holography. Since LEED $I(E)$ curves and Kikuchi patterns could be measured with standard reverse-view LEED optics, it is possible that surface structure determination, by using direct transform of LEED $I(E)$ curves as well as glancing Kikuchi electron patterns, in conjunction with STM, will become routine work in an ordinary laboratory.

To conclude, the integral-energy phase-summing method (IEPSM) is a simple method and easy to learn; in fact, to do the transform of diffraction patterns takes only a few minutes on a personal computer. We believe that the direct transform of diffraction patterns will soon become a powerful and widely used tool to study the surface structures.

Acknowledgement

We would like to acknowledge the financial support from the National Science Council of the Republic of China under the grants NSC 89-2112-M-007-075.

References

[1] Szoke A 1986 *Short Wavelength Coherence Radiation: Generation and Application (AIP Conf. Proc. 147)* ed D T Attwood and J Boker (New York: AIP)
[2] Barton J J 1988 *Phys. Rev. Lett.* **61** 1356 and references therein
[3] Saldin D K and de Andres P L 1990 *Phys. Rev. Lett.* **64** 1270
[4] Harp G R, Saldin D K and Tonner B P 1990 *Phys. Rev. Lett.* **65** 1012
[5] Barton J J 1991 *Phys. Rev. Lett.* **67** 3106
[6] Tong S Y, Li H and Huang H 1991 *Phys. Rev. Lett.* **67** 3102
[7] Wei C M and Tong S Y 1992 *Surf. Sci. Lett.* **274** L577
Wei C M, Tong S Y, Wedler H, Mendes M A and Heinz K 1994 *Phys. Rev. Lett.* **72** 2434
Saldin D K *et al* 1997 *Surf. Rev. Lett.* **4** 991
[8] Hong I H, Jeng P R, Shyu S C, Chou Y C and Wei C M 1994 *Surf. Sci. Lett.* **312** L743
[9] Abukawa T, Wei C M, Hanano T and Kono S 1999 *Phys. Rev. Lett.* **82** 335
[10] Chang C Y, Lin Z C, Chou Y C and Wei C M 1999 *Phys. Rev. Lett.* **83** 2580
[11] Van Hove M A, Weinberg W H and Chan C-M 1986 *Low-Energy Electron Diffraction* (Berlin: Springer)
[12] Luh D-A, Miller T and Chinag T-C 1998 *Phys. Rev. Lett.* **81** 4160 and references therein
[13] Wei C M, Hong I H and Chou Y C 1994 *Surf. Rev. Lett.* **1** 335
[14] Wei C M, Hong I H, Jeng P R, Shyu S C and Chou Y C 1994 *Phys. Rev.* B **49** 5109
[15] Chang C Y, Chou Y C and Wei C M 1999 *Phys. Rev.* B **59** 10 453
[16] Hong I H, Liao D K, Chou Y C, Wei C M and Tong S Y 1996 *Phys. Rev.* B **54** 4762
[17] Ahn H, Wu C-L, Gwo S, Wei C M and Chou Y C 2001 *Phys. Rev. Lett.* **86** 2818
[18] Nogami J 1994 *Surf. Rev. Lett.* **1** 395 and references therein
[19] Takahashi T, Nakatani S, Okamoto N, Ishikawa T and Kikuta S 1988 *Japan. J. Appl. Phys.* **27** L753
[20] Ding Y G, Chan C T and Ho K M 1991 *Phys. Rev. Lett.* **67** 1454
[21] Watanabe S, Aono M and Tsukada M 1991 *Phys. Rev.* B **44** 8330
[22] Ding Y G, Chen C T and Ho K M 1992 *Surf. Sci.* **275** L691
[23] Ranke W 1990 *Phys. Rev.* B **41** 5243
[24] Dabrowski J, Mussig H-J and Wolff G 1994 *Phys. Rev. Lett.* **73** 1660
[25] Knall J, Pethica J B, Todd J D and Wilson J H 1991 *Phys. Rev. Lett.* **66** 1733
[26] Jocobi K and Muler U 1993 *Surf. Sci.* **284** 223
Huang H, Tong S Y, Myler U and Jacobi K 1994 *Surf. Rev. Lett.* **1** 221

[27] Gai Zeng, Ji Hang, Gao Bo, Zhao R G and Yang W S 1996 *Phys. Rev.* B **54** 8593
[28] Vogler H, Iglesias A, Moritz W and Over H 1998 *Phys. Rev.* B **57** 2315
[29] Wang J, Horsfield A P, Pettifor S G and Payne M C 1996 *Phys. Rev.* B **54** 13 774
[30] Wei C M (calculated by VASP code, unpublished)
[31] Laracuente A, Erwin S C and Whitman L J *Phys. Rev. Lett.* **81** 5177
[32] Liu A Y and Cohen M L 1990 *Phys. Rev.* B **41** 10 727
Xu Y-N and Ching W Y 1995 *Phys. Rev.* B **51** 17 379
[33] Bauer E *et al* 1995 *Phys. Rev.* B **51** 17 891
[34] Wang X-S *et al* 1999 *Phys. Rev.* B **60** R2146
[35] Nishijima M *et al* 1984 *Surf. Sci.* **137** 473
[36] Morita Y and Tokumoto H 1999 *Surf. Sci.* **443** L1037
[37] Rottger B, Kliese R and Neddermeyer H 1996 *J. Vac. Sci. Technol.* B **14** 1051
[38] Kress G and Hafner J 1993 *Phys. Rev.* B **47** 558
Kress G and Hafner J 1994 *Phys. Rev.* B **49** 14 251
Kress G and Hafner J 1994 *J. Phys.: Condens. Matter* **6** 8245
[39] Zhao G L and Bachlechner M E 1998 *Phys. Rev.* B **58** 1887
Wang H *et al* 1999 *Surf. Sci.* **443** L1037
[40] Nakatani S, Kuwahara Y, Takahashi T and Aono M 1996 *Surf. Sci.* **357** 65
[41] Chen X, Abukawa T and Kono S 1996 *Surf. Sci.* **356** 28
[42] Martensson P, Meyer G, Amer N M, Kaziras E and Pandeay K C 1990 *Phys. Rev.* B **42** 7230
[43] Hong I H, Jih M J, Chou Y C and Wei C M 1997 *Surf. Rev. Lett.* **4** 733